Biocybernetics and Biomedical Engineering 44 (2024) 858–873

Contents lists available at ScienceDirect

Biocybernetics and Biomedical Engineering

journal homepage: www.elsevier.com/locate/bbe

Influence of 3D-printed cellular shoe soles on plantar pressure during running – Experimental and numerical studies

Paweł Baranowski [a,*], Aleksandra Kapusta [a], Paweł Płatek [b], Marcin Sarzyński [b]

[a] Military University of Technology, Faculty of Mechanical Engineering, Institute of Mechanics & Computational Engineering, 2 Gen. S. Kaliskiego Street, 00-908 Warsaw, Poland

[b] Military University of Technology, Faculty of Mechatronics, Armament & Aerospace, Institute of Armament Technology, 2 Gen. S. Kaliskiego Street, 00-908 Warsaw, Poland

ARTICLE INFO

Keywords:
Additive manufacturing
Cellular structure
FEA
Shoe sole
3D printing
TPU 95

ABSTRACT

The paper explores the potential of additive manufacturing (AM), experiments and simulations to develop a personalized shoe sole, with cellular topology used as the insert that minimizes the plantar pressure during running. Five different topologies were manufactured by Fused Filament Fabrication 3D printing technique using thermoplastic polyurethane TPU 95 filaments and tested experimentally and using FEA under compression conditions. The error between the maximum peak force and specific energy absorbed (SEA) from the model and experiment were less than 4.0 % and 6.0 %, respectively. A deformable FE foot model was developed, which was validated against data from the literature on balanced standing and the landing impact test carried out in the study. For the first case, the predicted maximum pressure (P_{peak} = 0.20 MPa) was positioned between the data presented in previous papers (0.16 MPa ÷ 0.30 MPa). In the second case, the experimentally measured and numerically predicted force peak values were nearly identical: 1760 N and 1720 N, respectively, falling with the range of 2.2 ÷ 2.5 BW similarly to other studies. Finally, a shoe sole design was proposed based on these topologies, which was simulated in the rearfoot impact to investigate the deformation of the sole and its influence on the foot plantar pressure peak and its distribution. The findings indicated that the sole with cellular structure could drastically reduce plantar pressure and improve overall footwear performance. This research provides valuable guidance and insights for designing, modelling, and simulating customized shoe sole manufactured using the 3D printing technique.

1. Introduction

There are two common runner types: forefoot and rearfoot. It was found that the second running style results in a higher vertical loading rate on a barefoot runner compared to other styles of foot strikes [2,3]. Furthermore, it was observed in [1] that the energy in the foot during rearfoot strike is much higher compared to forefoot striker. This was related to the fact that the main force is sustained by the heel pad. Regarding the shod runners, it was found that approximately 80–85 % of runners use rearfoot strike [4,5]. Therefore, it is clear that a proper design of the running shoe sole has a direct impact on running comfort and effectiveness of a training. Otherwise, the resulted high plantar pressure and high peak of impact energy can increase a risk of injury or foot diseases [1]. The modern technologies can improve the process of manufacturing high-performance footwear, and the popularity of additive manufacturing (AM) resulted in growing interest in this area [2–9] to develop shoes with midsoles built from a lattice or cellular structure, which have a low relative density, while providing good mechanical properties, including strength and/or damping.

Several studies have demonstrated the potential of 3D-printed midsoles featuring lattice or cellular designs using experimental or/and numerical simulations based on the finite element method (FEM) [2–4,6,8,10–21]. In the case of finite element analyses (FEA), a numerical model of foot is needed to credibly analyse the influence of sole on the plantar pressure [16,22–25]. However, in most of the papers, the foot is omitted or is treated a non-deformable. For instance, in, [21], Ma et al. adopted the AM technique to manufacture samples based on porous structural units and the final model of a diabetic insole with

* Corresponding author.
E-mail addresses: pawel.baranowski@wat.edu.pl (P. Baranowski), aleksandra.kapusta@student.wat.edu.pl (A. Kapusta), pawel.platek@wat.edu.pl (P. Płatek), marcin.sarzynynski@wat.edu.pl (M. Sarzyński).

https://doi.org/10.1016/j.bbe.2024.11.004
Received 9 September 2024; Received in revised form 26 November 2024; Accepted 26 November 2024
Available online 30 November 2024

gradient modulus; the FEM was also used but the authors omitted the foot in their investigations. In her thesis [2], E. Heiml, demonstrated a design method for shoe soles made of lattice structures printed with polyamide (PA12) and thermoplastic polyurethane (TPU). Unfortunately, the foot was not modelled in this study. Quite recently, Cheng et al. [19], proposed a 3D Voronoi strut midsole design based on plantar pressure distribution. In this paper, FEA is conducted but no information regarding the methodology for foot representation is given. On the other hand, Dong et al. [8], Mohamad et al. [4] and Zolfagharian et al. [3] tested 3D-printed shole midsoles made of a lattice structure under static loading conditions. They used simple midsole designs based on hexagonal, elliptical, circular and diamond topologies. Although the foot model was considered, it was treated as rigid. In contrary, a single-part deformable foot was used in [6] and [17]. In both papers, an optimization technique was employed to generate and manufacture the customized porous and foam-like shoe sholes via AM method.

While many scholars have analysed foot mechanics using static or quasi-static simulations, few papers aimed at analysis of foot deformation using explicit simulations. For example, Hannah et al., [26], proposed a numerical footstrike model based on kinematics conditions obtained from a motion capture. The foot was represented by rigid plates simulating phalangeal, metatarsal, and calcaneal segments of the foot. An alternative approach of modelling the footstrike proposed in the study was found to not efficiently reproduce the experimental trials. Another explicit analysis of barefoot strike (forefoot and rearfoot) was conducted in [27]. For this purpose, a detailed foot FE model was developed based on CT scanning and validated against experimental tests. During the simulations the stress level in the metatarsal was analyse and the potential injury due to the high stress level during landing phase was highlighted. A similar study for gait simulation was presented by Qian et al. [28]. The quasi-static as well as dynamic FE models of the foot were proposed using a 2D approach. Despite a simplified two-dimensional representation of the foot, promising results were achieved, and the model could be enhanced in future studies. A coupled foot-shoe-ground interaction model for explicit simulation of landing impact was proposed in [24] and [29]. Lower limp skeleton and soft tissue were simplified, but the four-part shoe was reproduced in detail. The landing simulation was performed assuming vertical impact against the ground. The model was validated using ground reaction force (GRF) histories obtained from experimental tests and FEA.

This paper aims to address current gaps by proposing a novel methodology that combines experimental tests and advanced FEM simulations to analyse the influence of different cellular midsole inserts on the plantar pressure values and distribution within a realistic foot model as well as on the observed reaction force during rearfoot strike. To the best of the authors' knowledge, this is the first paper in which a fully dynamic simulation of the foot landing scenario of foot / boot interaction with a ground during running was conducted, in which a deformable foot and a 3D printed cell shole were employed. From this paper, the following scientific and novel aspects can be distinguished: (1) implementation of AM technology to manufacture five different cellular topologies for the midsole; (2) validation of numerical models based on the experimental uniaxial compression tests, plantar pressure values and distribution (literature data), force plate test measurements, and (3) implementation of a deformable foot FE model considering the stiffness of a leg in a dynamic landing running scenario.

2. Materials and methods

2.1. Research methodology

The methodology consisting of four main stages adopted in this paper is presented in Fig. 1. The three first stages are divided into two parts: the first was focused on cellular topologies, whereas the second was focused on foot. In both stages, the goal was to develop credible numerical models to be used in the last, fourth stage of this study.

In the first stage, *Experiments*, five different cellular topologies were developed and 3D printed cubical specimens were manufactured using the Fused Filament Fabrication (FFF) technique with thermoplastic polyurethane TPU 95 (Thermoplastic Polyurethane with a Shore hardness of 95A) filament. These specimens were experimentally tested under quasi-static compression to analyse their deformations, force characteristics, and energy absorption properties. Simultaneously, the participant ran barefoot on the force plate and the reaction force was measured by the BTS P6000 platform, and a 3D laser scanning process was carried out to acquire outer geometry of the participant's left foot.

In the second stage, *Numerical modelling,* the numerical models of cellular topologies were developed, and a deformable foot FE model was proposed. The initial – boundary conditions for conducting validation analyses were specified, i.e. uniaxial compression tests for cellular topologies, and balanced standing and landing impact for FE foot model.

In the third stage, *Validation*, the numerical models of the topologies were simulated under identical conditions as in the experiments to quantitatively and qualitatively compare the results. Furthermore, the proposed deformable foot FE model was also validated against the literature data in balanced standing and based on the conducted force plate test in the first stage of this study.

In the last stage, *Sole design and simulations,* the validated numerical models of cellular topologies were used to design five shoe soles and the simulations of foot – sole impact (landing) into the ground reflecting rearfoot strike during running were conducted for each shoe sole. The influence of five different soles with previously tested topologies on the foot's plantar pressure distribution was analysed and the results were compared with the landing impact simulation using the barefoot discussed in stage no. 3.

2.2. Experiments

2.2.1. Manufacturing of cellular structures used for shoe sole

Five geometrical models of cube-shaped cellular topologies were designed with the same relative density as the shoe soles described in Section 2.4.1. The following structures were considered*: honeycomb, triangle, rhombic, squared,* and *re-entrant*. The *honeycomb* is a starting point for many studies of cellular structures [30,31], whereas *re-entrant* is a classic and the first example of the auxetic modification of *honeycomb* geometry [32]. Authors of several papers indicate that loading these structures in the in-plane direction results in the long-range plateau region on the force–deformation curve [33,34]. Other three topologies, i.e. *triangle, rhombic* and *squared* are the basic geometrical shapes. These and other topologies were previously used in similar studies [3,8]. Considering the future planned use of a material with hyperelastic properties, which allows for a high range of elastic deformation, it was decided to verify how the mechanical response of structures defined by simple geometric cells would behave. An additional factor influencing the choice of the shape of the unit cells was the technological feasibility of their production using 3D printing via the FFF technique. Simple unit cell shapes are easier to fabricate, both when manufacturing the structures and the sole [35,36]. Based on the geometrical models, the 3D printed, and their FE representations were prepared for quasi-static compression tests and simulations discussed in the next sections. The specimens had an identical depth and wall thickness of 30.0 and 1.0 mm, respectively, while height and width depended on the shape of a unit cell. All five cellular topologies had a relative density close to 0.3. Furthermore, minimum five unit cells were assumed in the height of the specimen according to the previous study [30,37,38]. Fig. 2 shows the 3D printed cubical specimens of the five 2D cellular topologies with marked dimensions and calculated relative densities.

As mentioned, PolyFlex TPU 95 (PolyMaker) material was used to manufacture the specimens. This material exhibits 95A Shore hardness, high flexibility, allowing the production of objects that can bend and stretch without breaking. This characteristic makes it ideal for

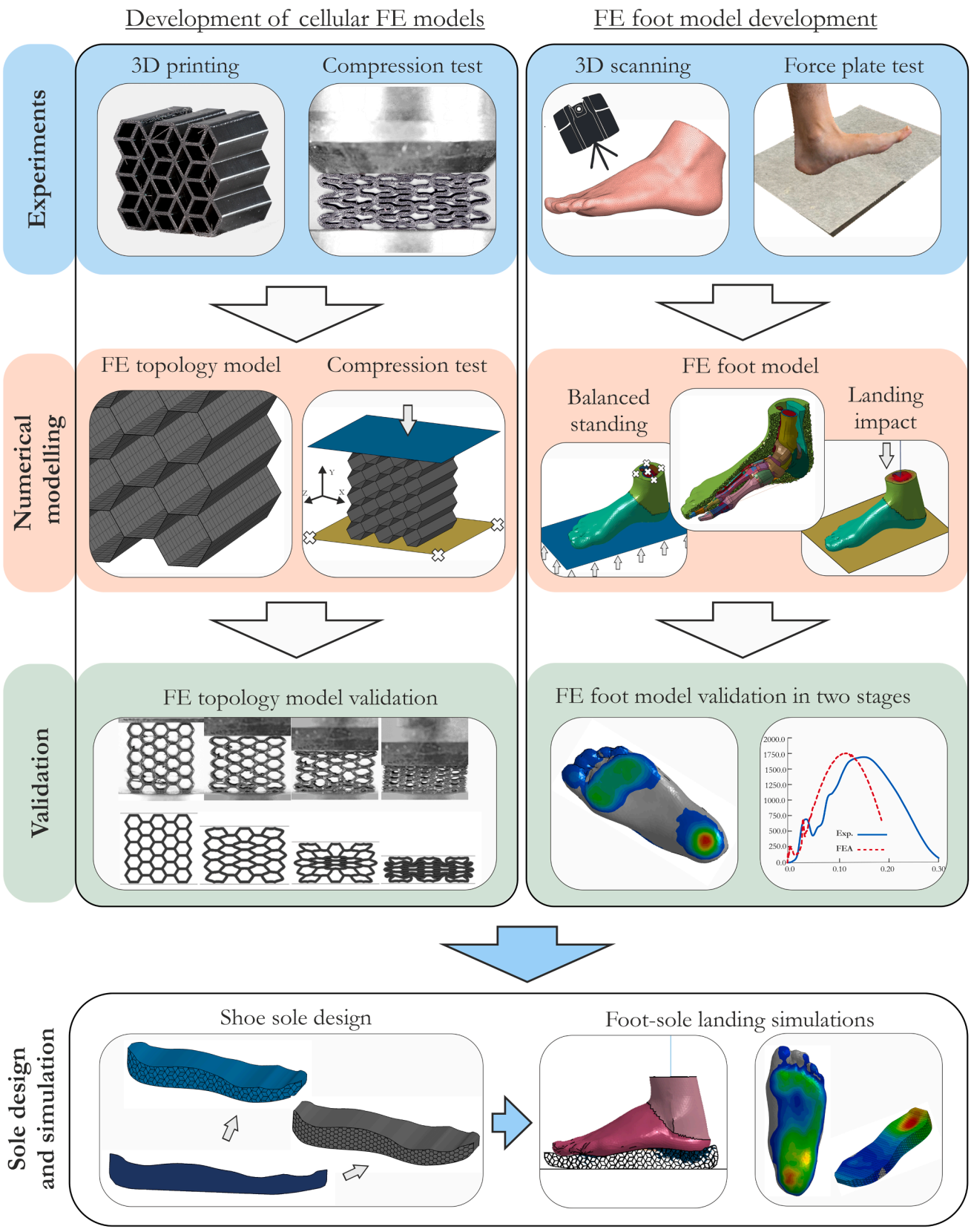

Fig. 1. Flow chart that presents the methodology of this study.

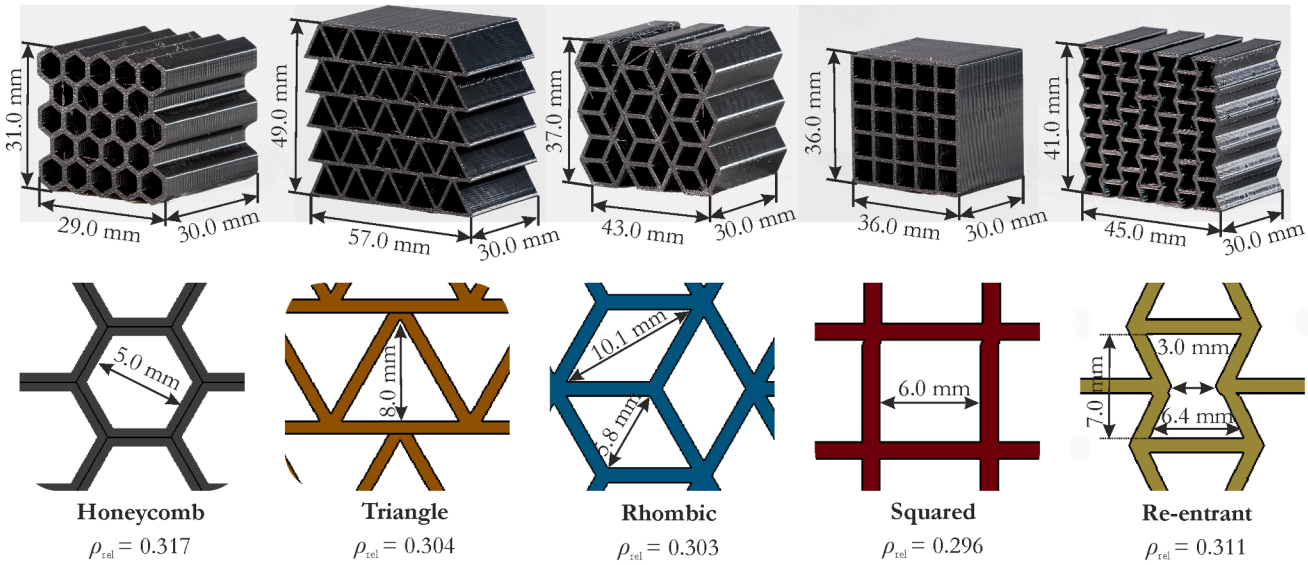

Fig. 2. The five cellular structures considered in the study with their geometrical dimensions.

applications that demand both durability and flexibility. Additionally, TPU 95 demonstrates excellent impact resistance, capable of absorbing shocks and impacts without cracking or permanently deforming. This makes it ideal for protective cases, bumpers, and other applications that require resilience. Furthermore, TPU 95 is known for its high resistance to wear and abrasion, making it an outstanding choice for parts subjected to friction or repetitive motion. TPU 95 is also easier to print because of its slightly higher hardness, compared to softer TPU materials. It is less prone to issues such as stringing, clogging, and deformation during 3D printing, making it more user-friendly for both beginners and experienced users. Among the flexible materials available on the market, TPU 95-Polyflex, offered by Polymaker Corp., was selected for this project. The mechanical properties of the filament used are presented in the accompanying in Table 1.

The 3D printing process was carried out using a 3D printer operating with FFF (Fused Filament Fabrication) technology, specifically the Prusa i3 MK3S+, offered by the Czech company Prusa Research. In the previous papers [39–41], the challenges associated with printing flexible and soft materials were highlighted. It was observed that the printing temperature has the most pronounced effect on the material hardness. Therefore, before proceeding with the production of test specimens, preliminary technological tests were conducted to select 3D printing parameters that would guarantee high geometric quality of the manufactured elements, as well as uniform material structure and minimal structural defects. The basic 3D printing parameters are presented below in Table 2. The identified parameters ensure proper adhesion of the TPU to the build plate and ensure that filament was properly melted and smoothly extruded through the nozzle.

Table 1
Mechanical properties of TPU 95 Polyflex material available on the producer website.

Density (ASTM D792)	Melt index (210 °C, 1.2 kg)	Elastic modulus (X-Y) ASTM D638	Tensile strength (X-Y) ASTM D638	Elongation at break (X-Y) ASTM D638	Shore hardness ASTM D2240
1.20–1.24	3–6 (g/10 min)	9.4 ± 0.3 (MPa)	29.0 ± 2.8 (MPa)	330.1 ± 14.9 (%)	95 A

2.2.2. Experimental compression tests of cellular structures used for shoe sole

Uniaxial and quasi-static compression tests were performed using the MTS Criterion C45.105 universal testing machine at a room temperature of 23 °C. The quasi-static compression test setup is shown in Fig. 3. The structures were tested in the in-plane orientation, i.e. the force is applied in the plane of the cross section through the cells of the structure. The samples (five for each topology) were placed between the flat and parallel surfaces of the brackets. Force values during the test were recorded using a force sensor with a range of 100kN. Additionally, the test course was recorded using a digital camera with a telephoto lens in order to compare the deformation form of the experimental samples with the results of the numerical simulation. TestSuite software is responsible for setting the compression test parameters and data acquisition. All topologies were compressed at a speed of 1 mm/s until a shortening of 50 % was achieved [30,31,42]. The proposed value for the structure deformation during tests was intended to prevent the full crushing of the structure, which could lead to densification and a significant increase in the deformation force. The authors aimed to evaluate the energy absorption of individual structural topology variants within the same deformation range, specifically where a plateau occurs. This approach to assessing the efficiency of structures in terms of energy absorption has been presented in the following publications [34,43]. The 50 % deformation is higher compared to remarks defined in the ISO 7743:2017 standard related to bulk thermoplastic rubber materials (the recommended range of deformation is 25 %). Nevertheless, the proposed methodology is usually adopted in many papers and in the present study it also gave correct results.

2.2.3. Force plate test: Barefoot running

The participant ran barefoot on the force plate and the reaction force was measured by the BTS P6000 platform. A foot strike test was conducted for each foot and the running trial was repeated five times; thus, ten trials were conducted overall. The measured force characteristics were used to validate the model and apply proper simulation conditions in the subsequent FEA (described in 2.3.3.2). The running speed was not monitored.

2.2.4. Foot geometry scanning process

To performs simulations of balanced standing and foot landing impact, an FE model of the left foot was acquired from THUMS (Total Human Model for Safety) [44]: a human body model reflecting internal

Table 2
3D printing parameters identified for TPU 95 Polyflex filament.

Nozzle temperature [°C]	Table temperature [°C]	Layer height [mm]	First layer height [mm]	Extrusion multiplier [-]	Printing speed [mm/s]
240	50	0.2	0.2	1.1	20

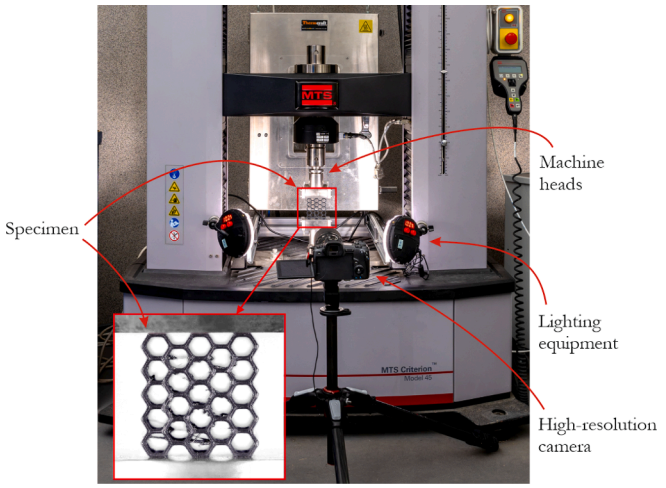

Fig. 3. Experimental setup for conducting quasi-static compression tests of the tested topologies.

organs, bones, muscles, etc., developed specifically for crash analyses. However, the original THUMS foot model was modified and the outer geometry (skin) of the participant's left foot was obtained by 3D laser scanning using the 3D SHINING3D EinScan Pro HD. The scanning process was carried out with the scan speed of 30 frames/s and 1,500,000 points/s and with the point distance of 0.2 mm. Ultimately, a point cloud consisting of 425,192 measurement points from the surface of foot object was obtained and the *.stl file was exported to construct the FE foot model described in Section 2.3.3.

2.3. Numerical modelling and simulations

2.3.1. Modelling and validation of the cellular structures used for shoe sole

To validate the modelling approach and the constitutive model used to represent the behaviour of the material in cellular structures, the FE models were developed using a similar methodology demonstrated in authors' previous papers [30,37]. For each model, shell elements with an average element size of approximately 0.8 mm were assumed. This element size was selected based on the mesh sensitivity study conducted for the representative model, i.e., rhombic topology. A penalty-based contact procedure was adopted to simulate the interaction between the parts. For interior contact within the topology and for rigid surface – specimen contact a friction coefficient of $\mu = 0.6$ was used [42]. Since the dynamic foot-sole-ground impact simulations (described in Section 2.4.1) were carried out using the explicit LS-Dyna solver, the quasi-static compression tests discussed here were also reproduced with this approach. The FE model of each specimen was inserted between two rigid walls to simulate the compression test. The bottom was fixed, while for the upper surface a prescribed velocity was defined according to Eq.1. Such an approach guarantees that the inertia effect is significantly minimised and at the same time gives the possibility of simulating quasi-static tests. This approach was effectively adopted in several previous studies [30,37]:

$$v(t) = \frac{\pi}{\pi - 2}\frac{s_{\max}}{T}\left[1 - \cos\left(\frac{\pi}{2T}t\right)\right] \quad (1)$$

where T is the simulation termination time and $S_{\max}$ is the final displacement of the rigid surface.

The TPU95 material was reproduced using a simple hyperelastic model, for which a stress vs. strain curve can be directly implemented based on the uniaxial tensile tests. Parameters were taken from the previous study [42], where an excellent reproduction of the specimen printed behaviour was presented. Therefore, correlation and validation of the selected model were skipped in this paper. The FE model of the representative topology (honeycomb) with initial boundary conditions is presented in Fig. 4.

2.3.2. FE foot modelling

A deformable FE foot model was based on the THUMS human body model [44]. However, the model was modified to mimic the foot of the participant. The outer geometry of the left foot was acquired by 3D laser scanning – discussed in Section 2.2.4. The skin in the original FE foot model from THUMS was removed and replaced by the scanned outer geometry of the actual foot, which was carefully positioned to position it correctly relative to the inner parts of the foot. Next, an original 3D soft tissue was removed, and a new one was constructed using tetragonal elements between the parts of the foot model: the scanned surface (skin) and the profundal fascia. Lastly, the plantar fascia represented using truss elements was also added, which improves the model's feasibility in terms of maintaining the proper biomechanical behaviour of the foot. It should be noted that the metatarsal and calcaneus geometries were not modified and were kept as original since the author did not perform computer tomography (CT) of the actual foot. The material properties of all components can be found in the THUMS documentation [44], however, a general information of the constitutive parameters and mesh properties of the foot components are listed in Table 3 and the FE model of the foot is shown in Fig. 5.

2.3.3. FE foot model validation

The numerical model of the foot was used to perform simulations with the following stages. First, a validation analysis of the model during standing was performed and the plantar pressure distribution was analysed and compared with the results of the available literature. Next, a barefoot landing simulation was carried out to reflect the platform testing procedure and validate the model in dynamic conditions.

2.3.3.1. Balanced standing. In Fig. 6, the foot model with appropriate initial boundary conditions used for simulating the balanced standing is presented. A 2D surface was used to reproduce the ground, which could only move vertically. For all nodes of the ground surface, a vertical force was applied, which value corresponded to half of the participant weight, that is, 34.0 kg. The foot–ground interaction was modelled using surface-to-surface contact with a friction coefficient of 0.6 [23,45,46]. The material properties of the ground were also taken from the literature [46]. Furthermore, the Achilles tendon force with the approximately 50 % of the force applied to the ground. This approach has been used effectively in the previous papers [16,23,45,46]. For this case, the implicit analysis was considered, and the plantar pressure distribution and peak values were analysed and compared with available literature data.

2.3.3.2. Landing impact. Since the dynamic problem was simulated, an explicit simulation was used to reproduce the landing on barefoot. The FE foot model was modified to mimic the impact of the foot on the

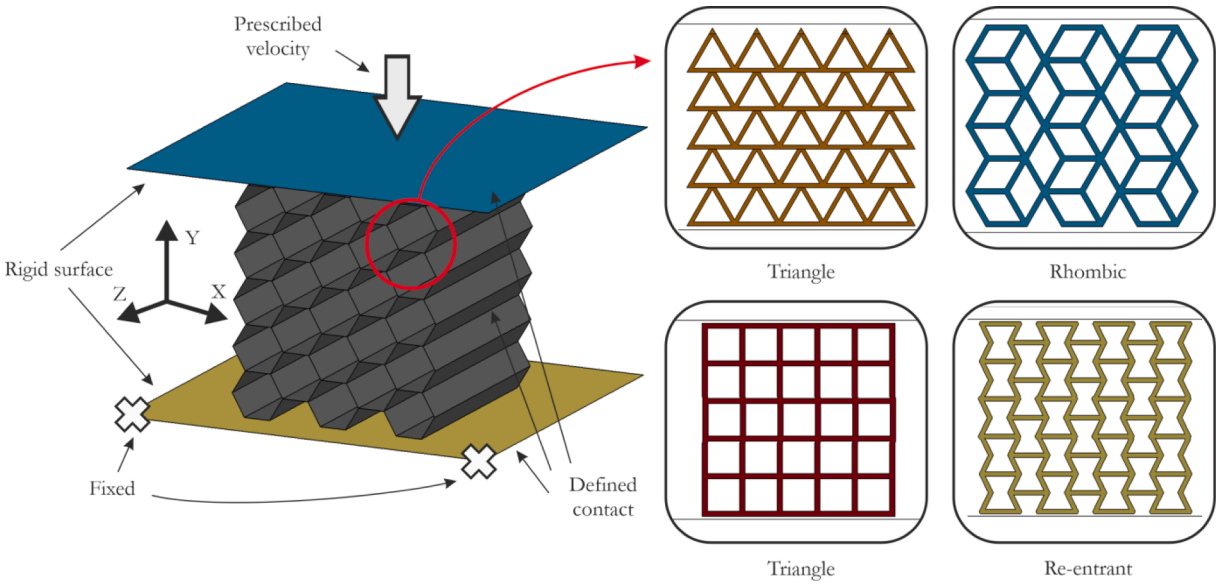

Fig. 4. Scheme of the representative numerical model (honeycomb) of cellular topologies with initial and boundary conditions.

Table 3
FE foot model data with mesh and constitutive models data.

Foot component	Type of element	Number of elements	Material model	Young's Modulus [MPa]	Poisson's ratio [-]	Density [kg/m^3]	Yield stress [MPa]
Trabecular bone	3D hexagonal	8633	Piecewise linear plasticity	15,000	0.3	2000	224.0
Cortical bone	3D hexagonal	1516	Elastic	73.4	0.45	1000	–
Soft tissue	3D tetragonal	321,536	Hyperelastic	Linear bulk modulus = 1000 MPa	0.495	1050	Stress vs. strain curve
Achilles tendon	3D hexagonal	211	Elastic	1200	0.4	1000	–
Skin	2D shell	8602	Fabric	11.0	0.3	1100	–
Profundal fascia	2D shell	3238	Null	1730	0.3	1000	–
Plantar fascia	1D truss	46	Elastic	350	0.4	1000	–
Ligaments	1D truss	81	Elastic	100	0.3	500	–

ground during the laboratory test on the force plate. The major modification was the implementation of a spring, with a length that corresponds to the participant's measured leg length equal to 903.0 mm. One of its ends was connected to the surface nodes of soft tissue, fibula, and distal tibia using rigid-body element. At the second end of the spring, a mass element was placed, which represented the participant's body mass of 68 kg. The stiffness of the spring representing the vertical stiffness was considered with a value of 25.0 kN (Fig. 7a). Since the speed of the participant during running on the force plate was not measured, this spring stiffness was determined based on the paper [47]. In this study, the spring mass characteristics were determined for elite and trained runners taking into account that: (1) the participant was a trained runner; (2) the measured reaction force value (F_{max}) during the force plate test was approximately 2.5 BW; (3) the vertical displacement (Δy) of the mass center was ~ 75 mm. Furthermore, the initial velocity $V_{initial} = 1700$ mm/s was specified for all parts in the model, based on the methodology proposed in the previous paper [24]. The ground was represented using a rigid wall and the friction coefficient between the foot and the ground was set to 0.6 [48]. The model discussed with the initial boundary conditions is shown in Fig. 7b.

2.3.4. Foot with sole landing: Design of the shoe sole and simulations description

For the simulation of landing impact with the shoe sole, the same model as in barefoot landing simulation was used. However, the sole with different topologies was used. A numerical model consisting of foot and sole with different topologies used as inserts was developed; in this stage, the influence of different topologies used for shole sole and its impact on the plantar pressure distribution were analysed. The interaction with the sole and the FE foot model was simulated using a penalty-based contact procedure with a friction coefficient equal 0.6 [48]. The foot-shoe sole model is presented in Fig. 7c.

The sole was designed for the left foot of the author (participant) of this paper with a European size shoe (EU) 42 (26.0 cm long). The shape of the sole was proposed based on a running shoe sold by the well-known athletic apparel and footwear corporation. However, its shape was modified taking into account the foot 3D scan data; therefore, a personalized shoe sole was developed and tested in this study. Five different inserts consisting of the investigated cellular topologies were used, and their numerical models are shown in Fig. 8. The wall thickness and relative densities were identical to those used in the quasi-static compression tests described earlier. Furthermore, the material data as the well as mesh size were also in agreement with the specimens simulated earlier.

3. Results

3.1. Compression tests of cellular structures used for shoe sole: experiments, FEA and validation

Quantitative and qualitative comparison of the experimental tests and FEA was performed. The force characteristics (reaction force versus

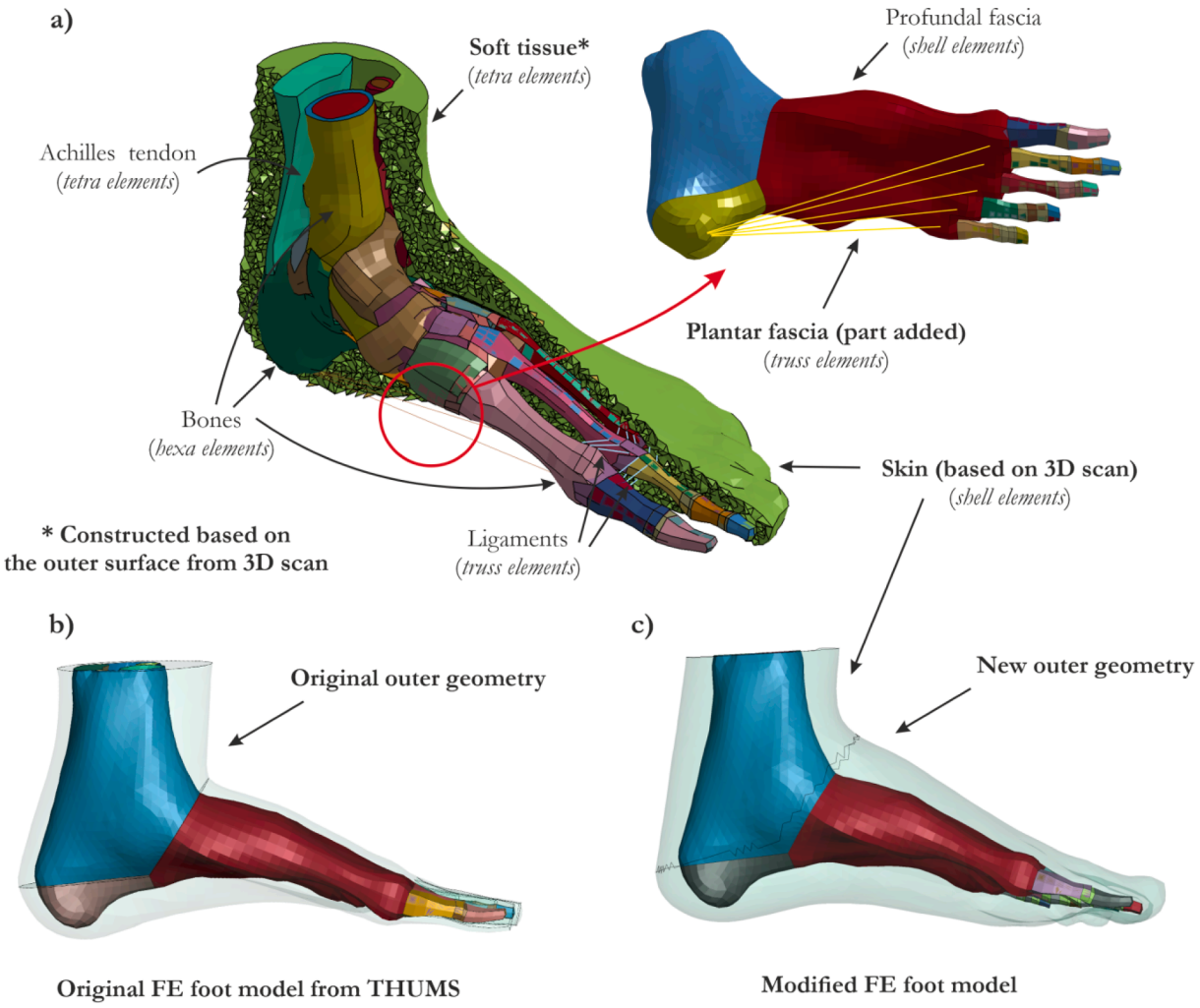

Fig. 5. a) FE foot model used for the numerical simulations in this study, b) original outer geometry from thums model, c) new outer geometry based on 3d scan.

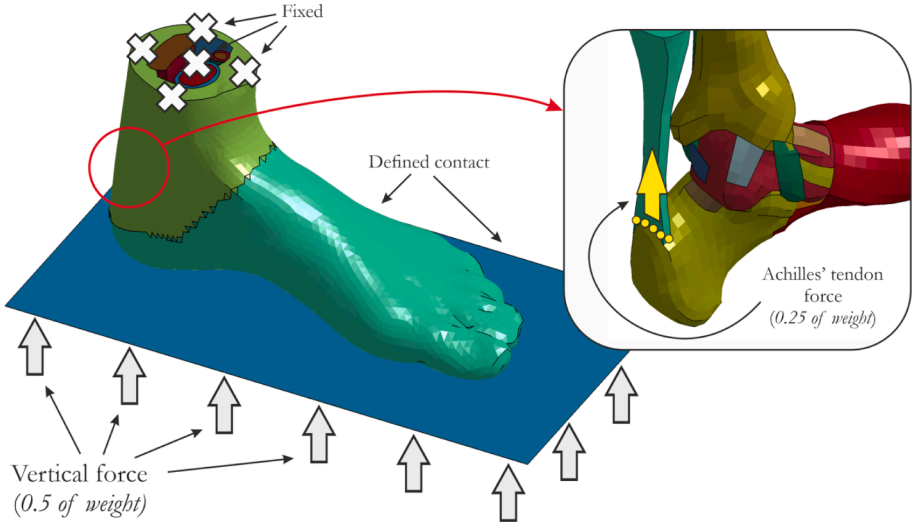

Fig. 6. FE foot model with initial boundary conditions for simulating the balanced standing.

strain) were analysed, which was followed by a comparison of the deformation process of the tested topologies. Moreover, energy absorption properties were also evaluated based on the obtained data.

Fig. 9a) shows the experimental force characteristics (averaged from five specimens for each topology) obtained by compression of the five topologies. For the three topologies, i.e. *honeycomb, triangle,* and *rhombic*, a stable force increase was observed, and the first two had the largest values of the forces during the whole period of deformation. For

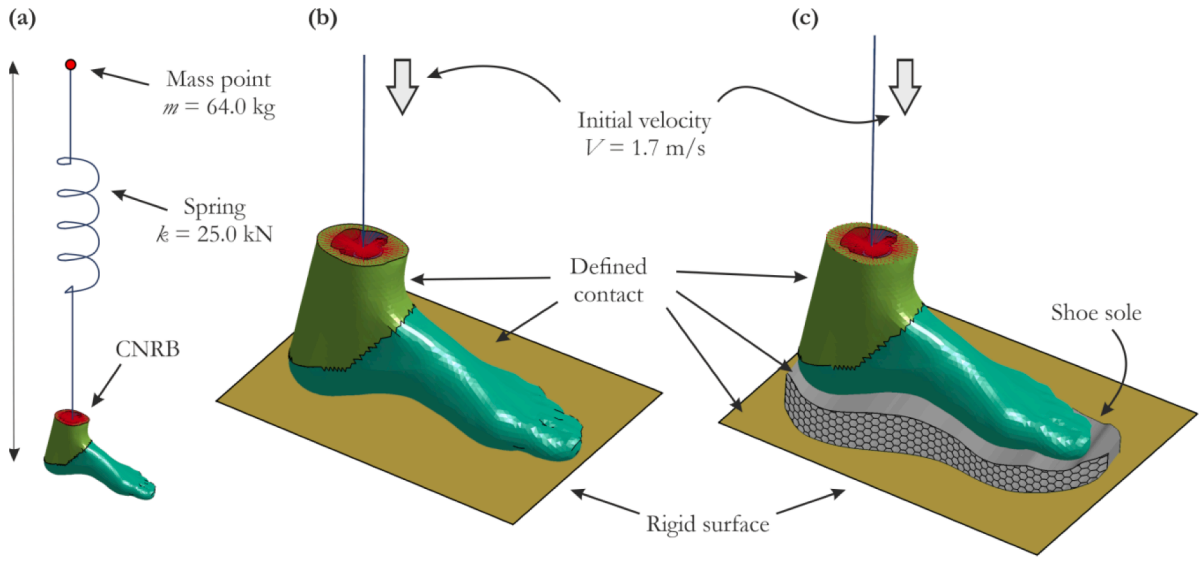

Fig. 7. FE foot model with initial boundary conditions for simulating the landing impact; (a) FE foot model with added spring and mass, (b) barefoot FE model and (c) FE foot with added shoe sole.

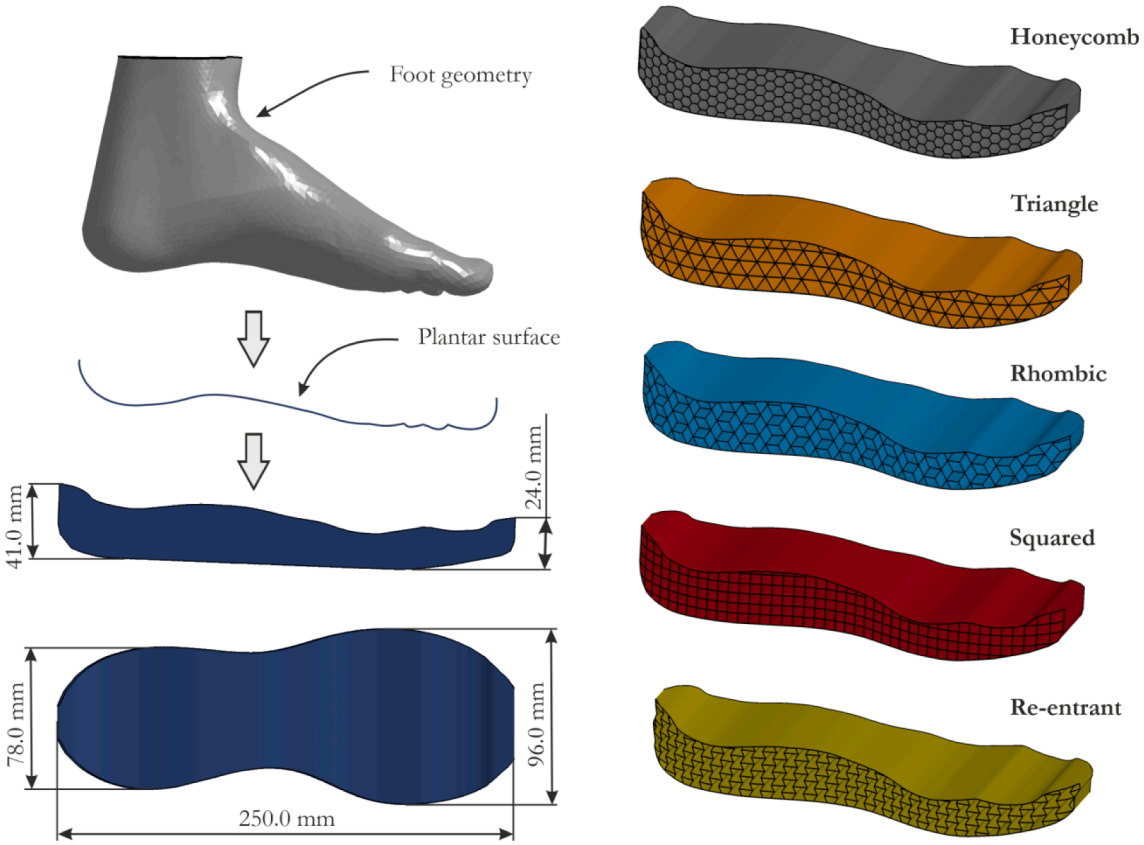

Fig. 8. Scheme of the shoe sole design and numerical models with different topologies used for the sole.

the *re-entrant* and *squared* topologies, the force characteristics were different compared to the other structures; after the first peak a visible plateau and significant force increase due to densification were observed. The smoothest and most stable curve was obtained for the *rhombic* and *honeycomb* topologies.

In Fig. 9b) – Fig. 9f), the force vs. strain obtained from laboratory tests and FEA are presented. Experimental results are represented by solid line, which is the average curve of all specimens. Furthermore, the standard deviation presented as a shaded zone are also included for each topology. In all cases, the numerical curve followed the experimental force measurement. The initial slopes of the curves from the numerical simulations correspond well with the actual force characteristic. A very good reproduction of force vs. strain characteristics was confirmed in the deformation process presented in Fig. 10. In all cases, four time-frames of the compression process were selected, for which the screen-shots from the camera and post-processor were included. The numerical

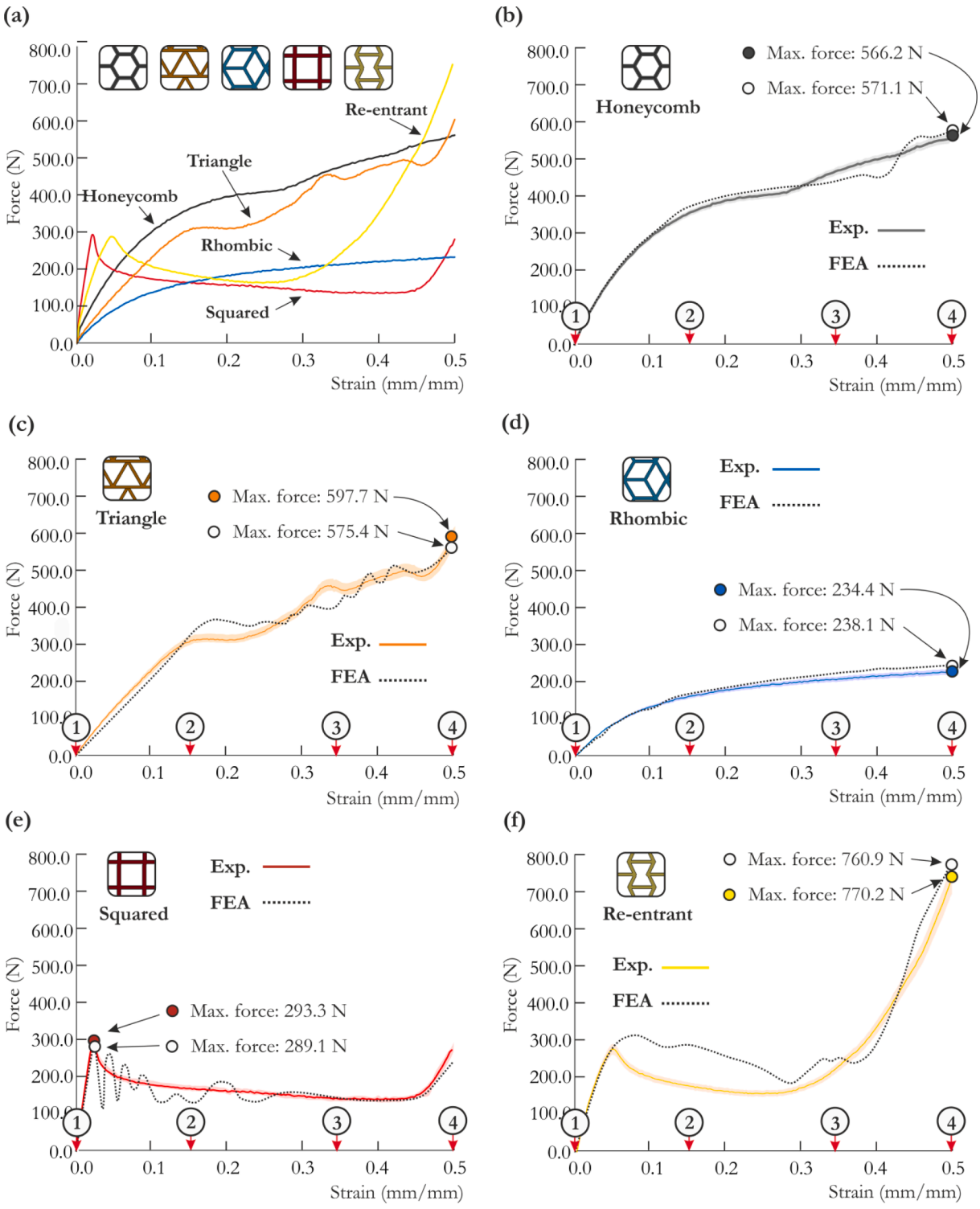

Fig. 9. Force vs. strain obtained from the quasi-static experimental compression tests (a) and comparison of force vs. strain curves from experimental tests and FEA for: (b) *honeycomb,* (c) *triangle*, (d) *rhombic*, (e) *squared*, (f) *re-entrant* topologies.

models for all topologies reproduced well the structure behaviour and force response, proving the credibility of the adopted constitutive model and discrete representation of the topologies.

The comparison between the experimental results and FEA as well as between the topologies is presented in Table 4.

3.2. FE foot model validation: Balanced standing and landing impact

Before simulating the rearfoot landing impact with the FE models of foot and shoe sole, the FE foot model was validated in the balanced standing test using the literature data and barefoot force plate test conducted by authors in the present paper. The plantar pressure was analysed and compared with experimental and FEA results. In Fig. 11a, the plantar pressure prediction of the current FE model is presented. The

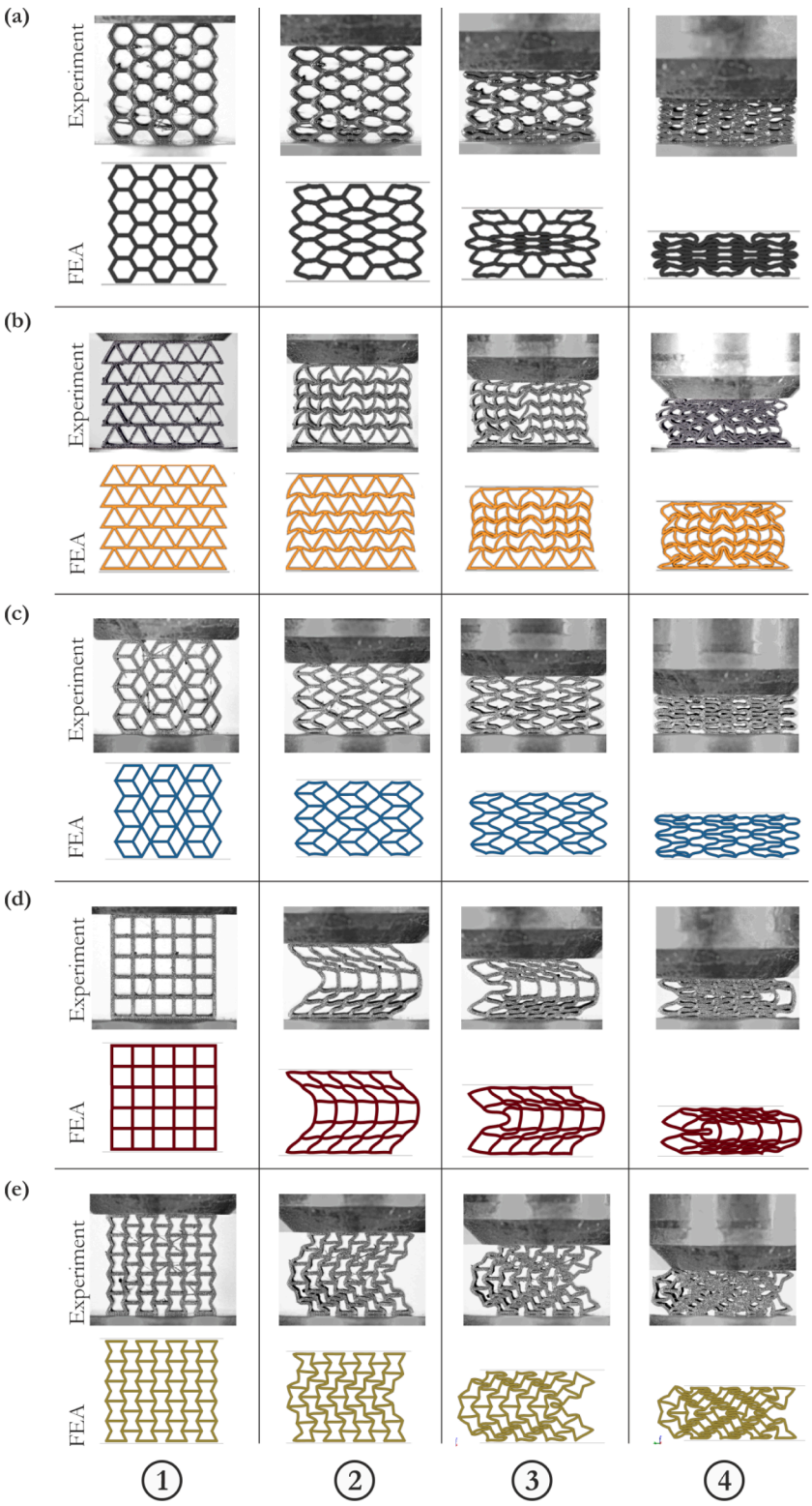

Fig. 10. Comparison of deformation process in experimental tests and FEA at selected stages of compression of the (a) *honeycomb,* (b) *triangle*, (c) *rhombic*, (d) *squared* and (e) *re-entrant* topologies.

maximum pressure of 0.200 MPa was located in the heel region, whereas the pressure below the metatarsal heads was lower with the maximum value of 0.132 MPa. A similar peak pressure in the heel region was obtained in [45] for the foot FE model (in this paper a participant with a body mass of 70 kg was also considered similar to the present paper). For other papers included in the comparison [49–51], a pressure peak between 0.160 – 0.170 MPa was observed in the heel region. In these papers participants had a body mass of 64 kg [49], 75 kg [50], and 80 kg [51].

In the next stage of validation, the force plate using the FE foot model test was simulated, and the force response of the barefoot was compared with the laboratory measurements described in Section 2.2.3. The foot

Table 4
Comparison of the experimental (mean values and standard deviations) and numerical compression tests results; difference are calculated based on mean values.

Type of topology	Exp. max. peak force [N]	FEA max. peak force [N]	Difference (FEA/EXP) [%]	Exp. SEA [J/kg]	FEA SEA [J/kg]	Difference (FEA/EXP) [%]
Honeycomb	566.2 ± 25.2	571.1	0.9	382.1 ± 16.9	386.6	1.2
Triangle	597.7 ± 38.1	575.4	−3.7	256.3 ± 18.1	251.4	−1.9
Rhombic	234.4 ± 16.6	238.1	1.6	325.4 ± 22.2	327.6	0.7
Squared	293.3 ± 22.4	289.1	−1.4	413.3 ± 31.3	419.2	1.4
Re-entrant	760.9 ± 43.3	770.2	1.2	262.8 ± 18.4	276.9	5.4

FE model (see Fig. 8b) was used and the rigid-wall reaction force history was obtained from this simulation. The force vs. time characteristics from experimental test and FEA are shown in Fig. 12. The peak forces were nearly identical and the curve shapes with initial force rises were obtained in the FEA and experimental results. However, the duration of the force was ~ 30 % shorter in numerical simulation compared to laboratory measurement. This is due to the different conditions of the FEA since only vertical movement of the leg was considered and a period of the running close to rearfoot striker was simulated. It should be also noted that the original FE foot model was previously validated and the results are discussed in detail in the THUMS model documentation [44].

3.3. Simulations of landing impact with shole sole made of cellular structures

Having validated models of the foot and cellular structures, numerical simulations of rearfoot landing impact test were carried out. As a reminder, identical conditions for the simulations were adopted as for the FE foot model validation in the force impact tests described above. Fig. 13 shows the force histories of the shoe soles with five topologies. The curves were limited to the moment of maximum measured force; therefore, the post-peak part of the curve was not presented. The displacement was measured for the point under the heel where the maximum deflection of the shoe sole was observed. The curves shown in the figure are not a reflection of those shown for the specimens in uniaxial compression (Section 3.1), due to their local nature this is because the maximum deflection in the sole under the heel was measured, not the global deformation of the entire sole. In Fig. 14, the plantar pressure distribution and the deflection of the shoe sole are shown for each topology. All topologies had an influence on foot pressure with a smaller peak pressure and a more homogeneous distribution compared to the case of barefoot, which is shown in Fig. 14f.

The comparison of shole sole deformation for all topologies is presented in Fig. 15. For the sake of a better visualization of the results the cross section of the shoe sole is shown. The deformation is more pronounced under the calcaneus area than the metatarsal part of the foot. This is attributed to the conditions of the simulations reflecting the rearfoot striker period of the running. The *squared* sole had much less pronounced deformation of the topological cells, compared to the other four topologies. However, in all cases bending and compression of the cell walls were observed as a result of foot pressing into the sole.

To analyse which topology absorbed more energy during landing, the internal energy was measured through structural deformation. Fig. 16 compares the SEA values of the five shoe soles. The presented data are not reflected in the maximum deflection of the heel region shown in Fig. 13 since in this case the data refer to the deformation of the

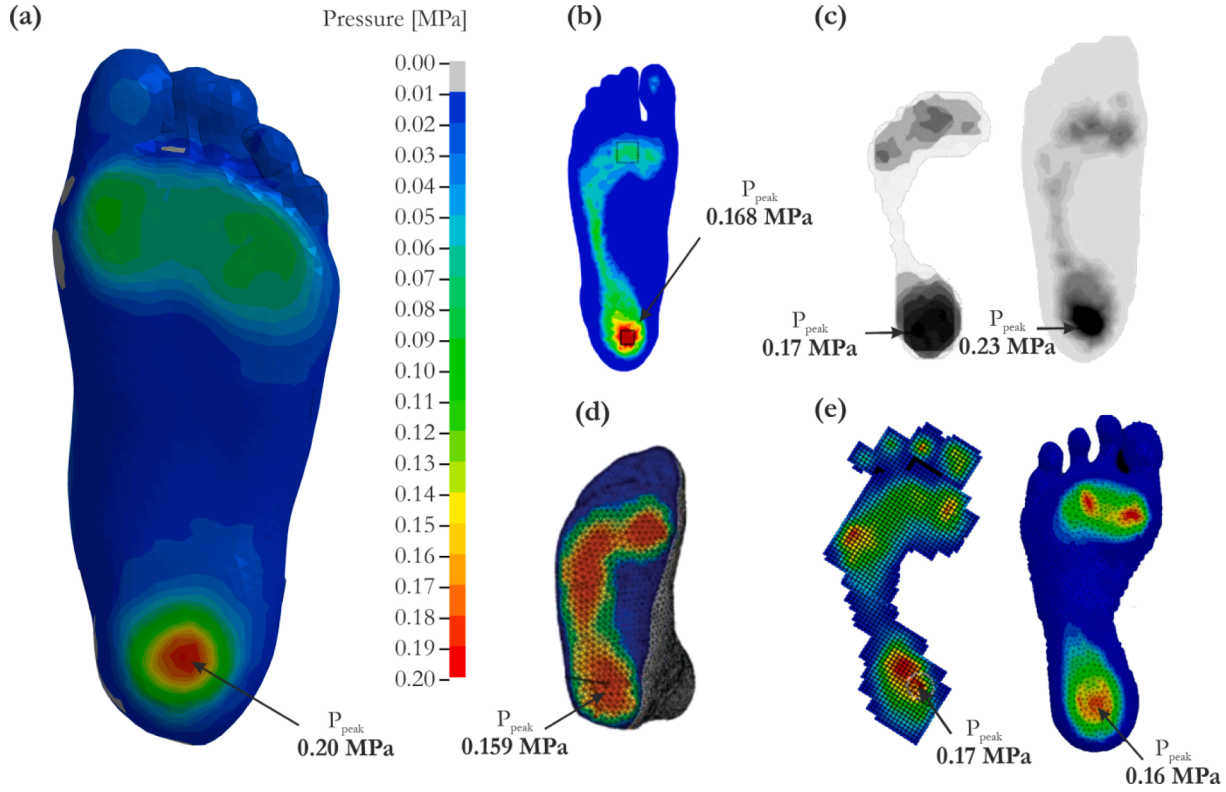

Fig. 11. Prediction of plantar pressure of the current model during balanced standing and comparison with published results using FEA and experiments: (a) Foot FE model in this study, (b) Wang et al., 2015 [49], (c) Cheung et al., 2005 [45], (d) Ozen et al., [51], (e) Antunes et al., [50].

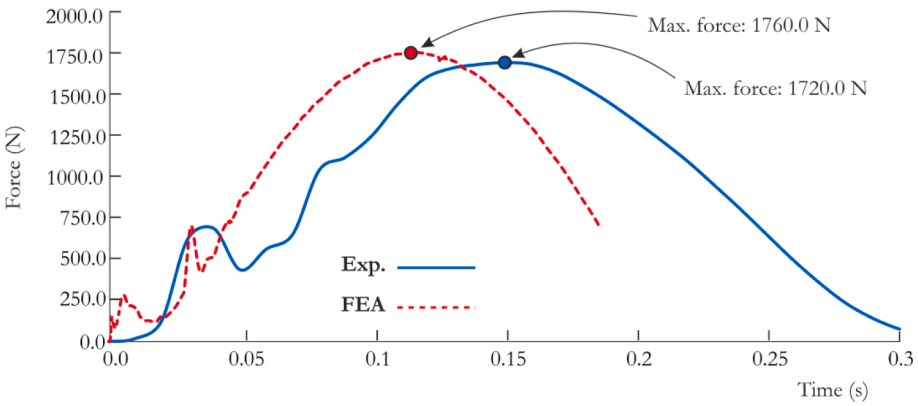

Fig. 12. Comparison of force vs. time curves for the force plate test obtained from experimental tests and FEA for the barefoot.

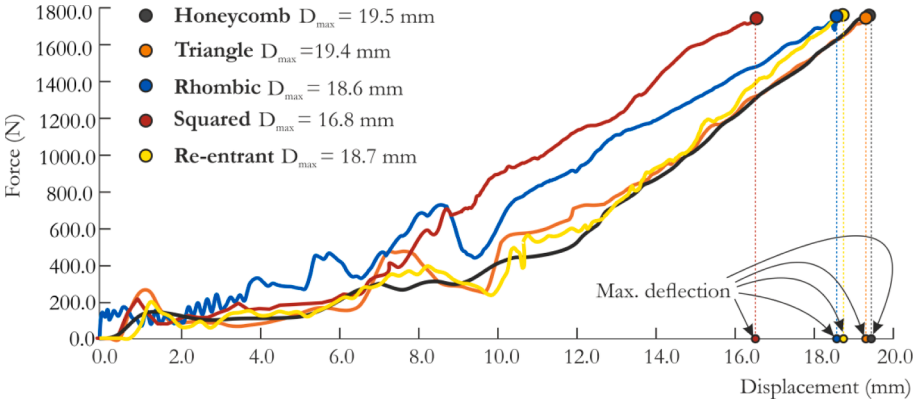

Fig. 13. Comparison of force vs. displacement (maximum deflection of the sole under the heel) curves for the landing impact test obtained from the FEA for five different topologies used for shoe sole.

whole sole structure, and not to the local region under the heel. For the *honeycomb* and *triangle* topologies, similar SEA was observed (24.1 J/kg and 24.6 J/kg). The *rhombic* and *squared* soles had larger values of SEA compared to the other three (28.4 J/kg and 28.6 J/kg, respectively). The shoe sole with *re-entrant* topology had the lowest SEA equal to 21.3 J/kg. The calculated SEA values, peak pressure values, max deflection within heel region, and pressure distributions are collated in Table 5. In this table, weight of each shoe sole was also included: the smallest weight was calculated for the *squared* sole (235 g), whereas the largest was obtained for the *re-entrant* sole with the weight of 249 g.

4. Discussion

This study focused on the simulation of the foot landing impact scenario during running, with the main emphasis pointed on the influence of different 2D cellular topologies used for the shoe sole on the plantar pressure distribution in the foot. The FFF 3D printing technique with TPU 95 material was utilized and five different structures were manufactured. Such a methodology using this type of filament has previously been adopted [6,17,52]. The topologies were experimentally tested under compression, followed by FEA to mimic the testing procedure. The numerical representation of all topologies was in good agreement with the outcomes from experimental tests. For the *re-entrant* topology, the discrepancy between the numerical and experimental force histories was more pronounced compared to the other topologies. However, the discrepancy between the FEA and experiment was not larger than 4.0 % regarding the maximum peak force. The closest agreement was obtained for the *honeycomb* (~1.0 % of error), while the largest discrepancy was calculated for the *triangular* topology with the maximum force value underestimated by 3.7 %.

In the studies of FE foot modelling with boot/ground interaction, one of the most significant parts is to properly reproduce the foot, which is a quite complex structure to be represented using FEM or other numerical technique. Numerous FE foot models have been proposed so far, with various complexities and assumptions [25,29,46,53]. The basic test to validate the numerical model of a foot is balanced standing, in which the reproduced plantar pressure is validated against the experimental measurement. The validation process is usually carried out by qualitative comparison of the pressure distribution [45,46,49–51,54,55] or/and measured peak pressure values [45,50,56,57]. The predicted pressure distribution was similar to several papers [12,58] and the maximum pressure value obtained for the present FE foot model was positioned between the data presented by other scholars. For example, in [49–51,58] the peak pressure varied between 0.159 MPa – 0.171 MPa, while in [27,45,57] the values of pressure were within the range of 0.204 MPa – 0.300 MPa.

Although in most cases similar participants' weights and foot size were considered, the predictions of pressure values as well as distribution in the FEA were different. There are several factors affecting the feasibility of the foot numerical model and, in consequence, resulting in different outputs of the models. Most importantly, the FE model can be sensitive to material properties, as was pointed out in previous papers [45,46]. Moreover, different outcomes can be observed depending on the assumptions considered and complexity of the modelling approach. Based on the above, the present foot FE model was considered as correct and feasible enough to be used in simulations of dynamic impact scenarios discussed in Section 3.2.

The results of these simulations and experimental tests are shown in Fig. 12 and the maximum force value in FEA correspondent well to experimental data. Initial impact and propulsive peaks were captured by

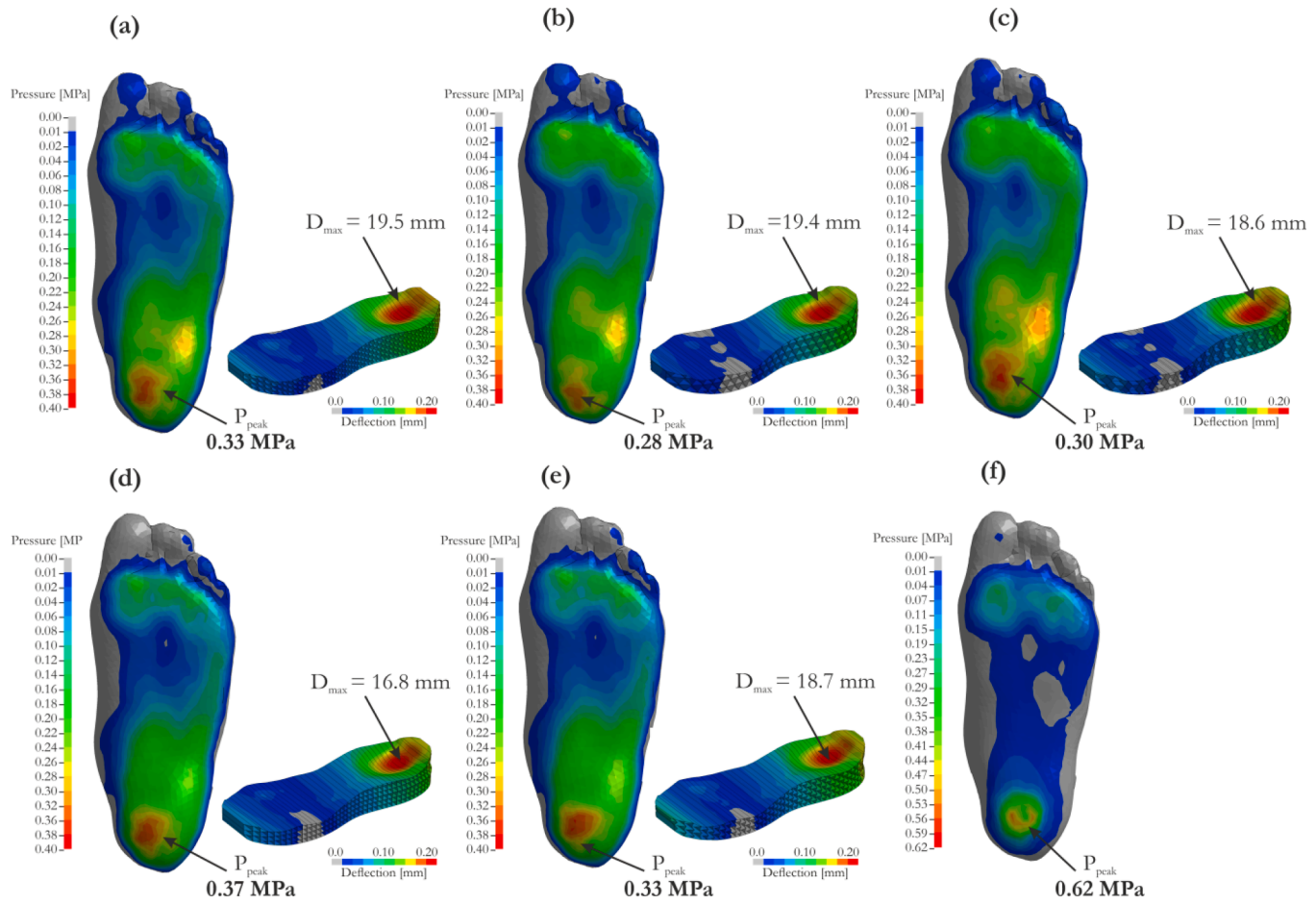

Fig. 14. Comparison of plantar pressure prediction of the model for the shoe sole with (a) *honeycomb,* (b) *triangle*, (c) *rhombic*, (d) *squared*, (e) *re-entrant topologies,* and (f) barefoot.

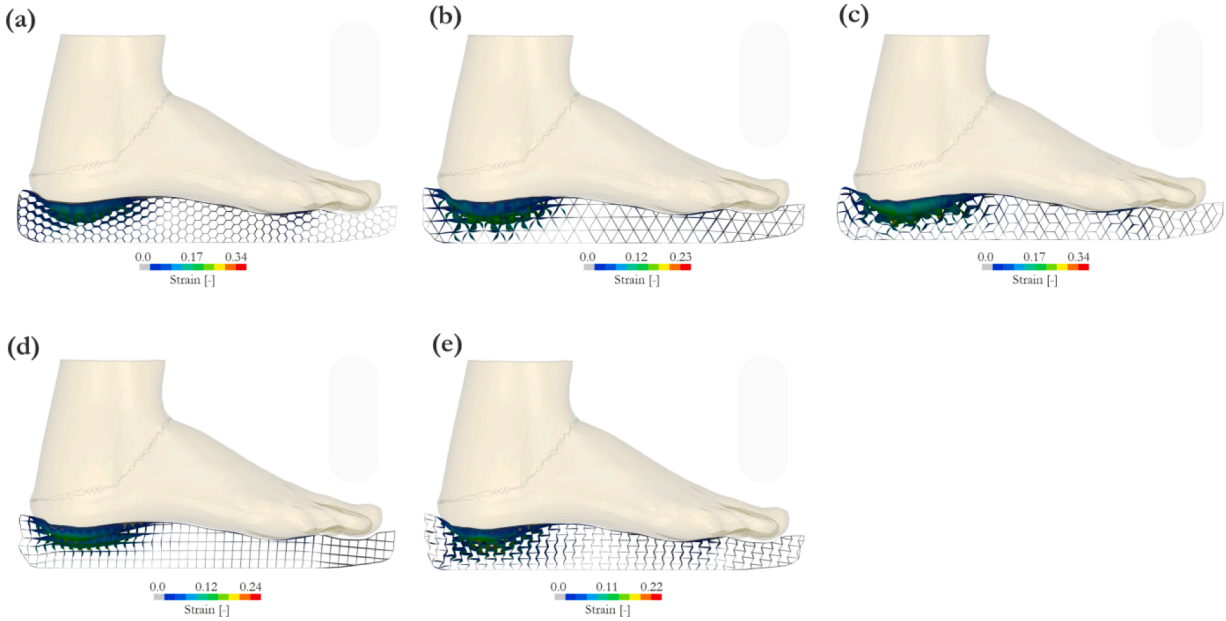

Fig. 15. Comparison of deformations and strain distributions of shoe sole with (a) *honeycomb,* (b) *triangle*, (c) *rhombic*, (d) *squared*, (e) *re-entrant* topologies.

the FE model. On the other hand, the duration of the force was shorter compared to the laboratory measurement – a similar observation can be found in [26]. It is worth noticing that the observed vertical GRF was similar to other studies [26,47,59,60], which generally falls within the range of 2.2–2.5 BW. When simulating the impact of the foot-shoe sole, a different effect on force response and the peak pressure distribution was

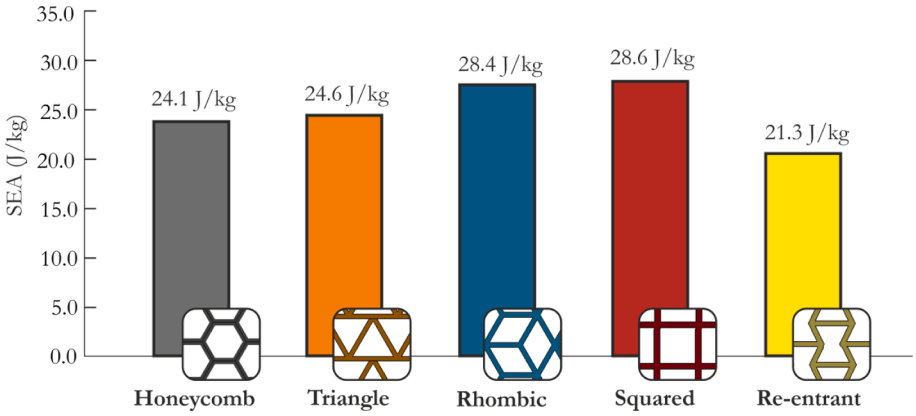

Fig. 16. Comparison of the absorbed energy (normalized to mass) of the five shoe soles.

Table 5
Results collation of landing impact simulations with different topologies used for the sole impact.

Topology used for the sole	Max. deflection under the heel [mm]	Max. peak pressure under the heel [mm]	Pressure distribution [-]	Specific Energy Absorbed [J/kg]	Weight of the shoe sole [kg]
Honeycomb	19.5	0.33	Fair	24.1	0.242
Triangle	19.4	0.28	Good	24.6	0.245
Rhombic	18.6	0.30	Good	28.4	0.242
Squared	16.8	0.37	Localized	28.6	0.235
Re-entrant	18,7	0.33	Localized	21.3	0.249

observed depending on the topology used for the insole. All shoe soles had a similar course of force vs. heel displacement curves, and the most stable characteristic was obtained for the *honeycomb* topology (Fig. 13). The stiffest topology was *squared,* $D_{max} = 16.8$ mm, while the *honeycomb* and *triangle* soles had the maximum deflection for the maximum force ($D_{max} = 19.5$ mm and $D_{max} = 19.4$ mm). One can notice that the forces correspond to the maximum force measured in the force plate test; however, their maximum values were captured for the deflection of the heel part of the sole in each case. The plantar pressure distribution obtained for each topology was compared with the barefoot simulation discussed above (see Fig. 14). The results are in good correspondence with the forces histories discussed above. The smallest and largest heel peak pressures were observed for the *triangle* (0.28 MPa) and *squared* (0.37 MPa) topologies, respectively. For the *honeycomb* and *re-entrant* similar value of peak pressure was obtained equal to 0.33 MPa. The sole with *rhombic* topology gave a heel pressure peak close to 0.30 MPa. In all cases, the heel peak pressure decreased approximately two times compared to the barefoot strike, for which a value of 0.62 MPa of the peak pressure was obtained (notably in [48] values between 0.509 MPa and 0.912 MPa were observed). The most homogeneous pressure distribution was obtained for the *rhombic* and *triangle* topologies, since the peak pressure within the heel was not so concentrated in these soles compared to other cases. Adding to this, reduced plantar pressure can minimise the risk of running injury [48]. The results showed that the *rhombic* shoe sole is the most promising, since it led to a small peak planar pressure and the most homogeneous pressure distribution while ensuring satisfactory sole stiffness.

There are some limitations of the present study. Although the FE model of the foot with deformable properties was included, there were some limitations connected to this. The metatarsal and calcaneus geometries were identical as in the original THUMS model. The authors did not perform CT of the actual foot. This could have an influence on the obtained results. The muscle forces were also not considered during both balanced standing and landing impact simulations. Therefore, their effect on foot behaviour were not reflected. However, by adding the plantar fascia and the force applied on the Achilles' tendon, satisfactory results were achieved. Furthermore, the present paper focused mainly on the analysis of a different shoe sole on the plantar pressure distribution. To achieve this, a deformable FE foot model was needed, which, in fact, was validated against two loading scenarios, proving its fidelity for the adopted studies included in this paper. The implemented model of the foot from THUMS can be relatively easily re-used by other researchers. Since it is not as complex compared to similar models proposed by other scholars [16,48,61], it has a rational computational cost with satisfactory efficiency. The second limitation is related to the landing impact conditions discussed in Sections 2.3.3, 3.2 and 3.3. Several scholars modelled the human foot during walking [11,46,62] and a rotation of angle with movement of the ground was imposed in their simulations. Similar conditions occur during running, where the foot rotates, and horizontal body velocity force the movement of the foot with respect to ground. In the present paper only the foot vertical velocity of the leg was simulated just as in the previous study [24]. This has led to ~ 30 % shorter duration of the force curve in the numerical simulation compared to the laboratory measurement (see Fig. 12). However, in FEA, the curve shape was similar, and the peak force was nearly identical compared to that observed in the experiment. Thus, a rearfoot strike period of the running was assumed in the simulations. Lastly, the study was conducted for only one participant and conditions of the test. Therefore, a larger number of participants and other running parameters (velocity, type of runner, etc.) should be considered for a wider and more general interpretation of the results [61].

5. Conclusions

In this paper, different 3D printed cellular topologies were employed for the shoe sole to analyse their influence on foot plantar pressure distribution during foot strike while running. Five different cellular topologies were manufactured using the material extrusion (MEX) technique with TPU 95 material. The obtained specimens were experimentally tested to analyse their deformation process and validate the following numerical modelling. The experimental tests were reproduced well by the proposed model. The shoe sole design was proposed, and the tested topologies were used as the sole filling and the foot-shoe sole rearfoot strike was simulated to assess how the different structure of the distribution of sole influenced the plantar pressure. For this purpose, a deformable FE foot model was used, which was validated against the static standing literature data and the impact test conducted under the scope of this study.

This study introduces a novel approach combining experimental tests, advanced numerical simulations and 3D printing technologies to provide a new insight for shoe designers and manufacturers.

Comfortable shoes with high-performance soles are desirable especially for runners, who seek optimized shoes that minimize the risk of potential injuries. Based on the outcomes shown in the present paper, it was demonstrated that the *rhombic* shoe sole provided good results in terms of pressure peak and its distribution as well as optimum sole stiffness, so it could reduce the probability of injury during running caused by the high-pressure concentration.

In the future, it is planned to extend the study to consider a larger number of participants and to manufacture the sole and test it under real-world conditions. Other topologies, i.e. 3D lattice, and different 3D printing techniques (e.g. FFF, SLS, SLA) and materials will also be taken into consideration.

CRediT authorship contribution statement

Paweł Baranowski: Writing – review & editing, Writing – original draft, Visualization, Validation, Supervision, Resources, Project administration, Methodology, Investigation, Funding acquisition, Conceptualization. **Aleksandra Kapusta:** Writing – original draft, Methodology, Investigation, Conceptualization. **Paweł Płatek:** Writing – review & editing, Software, Resources, Investigation, Conceptualization. **Marcin Sarzyński:** Investigation, Data curation.

Declaration of competing interest

The authors declare that they have no known competing financial interests or personal relationships that could have appeared to influence the work reported in this paper.

Acknowledgments

This research was supported by the Military University of Technology (Grant No. 22-717). This support is gratefully acknowledged. The numerical models were prepared using Altair HyperMesh software.

References

[1] Lieberman DE, Venkadesan M, Werbel WA, Daoud AI, Andrea SD, Davis IS, et al. Foot strike patterns and collision forces in habitually barefoot versus shod runners. Nature 2010;463:531–5. https://doi.org/10.1038/nature08723.
[2] Heiml E. Development of a Design Approach for Individualised 3D-Printed Cellular Polymeric Shoe Soles. Johannes Kepler University Linz; 2021.
[3] Zolfagharian A, Lakhi M, Ranjbar S, Bodaghi M. Custom shoe sole design and modeling toward 3D printing. Int J Bioprinting 2021;7(1–10). https://doi.org/10.18063/ijb.v7i4.396.
[4] Mohamad MR, Daud NA. The effect of sole design on foot stress distribution to runner. J Hum Centered Technol 2023;2(35–40). https://doi.org/10.11113/humentech.v2n2.54.
[5] Amza C, Zapciu A, Popescu D. 3D-Printed shoe last for bespoke shoe manufacturing. MATEC Web Conf 2019;290:1–6. https://doi.org/10.1051/matecconf/201929004001.
[6] Xie J, Zhou Z, Luo T, Pang H, Meng X, Zhou F. Study on design and additive manufacturing of customized bionic sports sole for the elderly. IEEE Access 2021;9:69830–8. https://doi.org/10.1109/ACCESS.2021.3078162.
[7] Silverman J. Development and Testing of Mycelium-Based Composite Materials for Shoe Sole Applications. University of Delaware; 2018.
[8] Dong G, Tessier D, Zhao YF. Design of shoe soles using lattice structures fabricated by additive manufacturing. Proc Int Conf Eng Des ICED 2019;2019-Augus:719–28. 10.1017/dsi.2019.76.
[9] Restrepo D, Mankame ND, Zavattieri PD. Programmable materials based on periodic cellular solids. Part I: experiments. Int J Solids Struct 2016;100–101:485–504. https://doi.org/10.1016/j.ijsolstr.2016.09.021.
[10] Low JH, Chee PS, Lim EH, Ganesan V. Design of a wireless smart insole using stretchable microfluidic sensor for gait monitoring. Smart Mater Struct 2020;29. 10.1088/1361-665X/ab802c.
[11] Shih KS, Jhou SY, Hsu WC, Hsu CC, Chen JW, Yeh JC, et al. A biomechanical investigation of athletic footwear traction performance: Integration of gait analysis with computational simulation. Appl Sci 2020;10. https://doi.org/10.3390/app10051672.
[12] Wang D, Li Z, Dey N, Ashour AS, Moraru L, Simon Sherratt R, et al. Deep-segmentation of plantar pressure images incorporating fully convolutional neural networks. Biocybern Biomed Eng 2020;40:546–58. https://doi.org/10.1016/j.bbe.2020.01.004.
[13] Nishiwaki T, Nonogawa M. Application of topological optimization technique to running shoe designing. Procedia Eng 2015;112:314–9. https://doi.org/10.1016/j.proeng.2015.07.251.
[14] Hsu YC, Gung YW, Shih SL, Feng CK, Wei SH, Yu CH, et al. Using an optimization approach to design an insole for lowering plantar fascia stress - a finite element study. Ann Biomed Eng 2008;36:1345–52. https://doi.org/10.1007/s10439-008-9516-x.
[15] Spahiu T, Almeida H, Ascenso RMT, Vitorino L, Marto A. Optimization of shoe sole design according to individual feet pressure maps. Comput Ind 2021;125:103375. https://doi.org/10.1016/j.compind.2020.103375.
[16] Song Y, Cen X, Zhang Y, Bíró I, Ji Y, Gu Y. Development and validation of a subject-specific coupled model for foot and sports shoe complex: a pilot computational study. Bioengineering 2022;9. https://doi.org/10.3390/bioengineering9100553.
[17] Xu J, Tu Z, Zhang S, Tan J, Wang G. Customized design for ergonomic products via additive manufacturing considering joint biomechanics. Chinese J Mech Eng Addit Manuf Front 2023;2:100085. https://doi.org/10.1016/j.cjmeam.2023.100085.
[18] Zhou Q, Niu W, Yick KL, Gu B, Sun Y. Numerical simulation of the effect of different footwear midsole structures on plantar pressure distribution and bone stress in obese and healthy children. Bioengineering 2023;10. https://doi.org/10.3390/bioengineering10111306.
[19] Cheng H, Liu B, Liu M, Cao W. Design of three-dimensional Voronoi strut midsoles driven by plantar pressure distribution. J Comput Des Eng 2022;9:1410–29. https://doi.org/10.1093/jcde/qwac060.
[20] Rico-baeza G, Gerardo IP, Alberto L, Cuan-urquizo E, Camarillo-g KA. Additively manufactured foot insoles using body-centered cubic (BCC) and triply periodic minimal surface (TPMS) cellular structures. Appl Sci 2023;13:12665. https://doi.org/10.3390/app132312665.
[21] Ma Z, Lin J, Xu X, Ma Z, Tang L, Sun C, et al. Design and 3D printing of adjustable modulus porous structures for customized diabetic foot insoles. Int J Light Mater Manuf 2019;2:57–63. https://doi.org/10.1016/j.ijlmm.2018.10.003.
[22] Cheung JTM, Zhang M. A 3-dimensional finite element model of the human foot and ankle for insole design. Arch Phys Med Rehabil 2005;86:353–8. https://doi.org/10.1016/j.apmr.2004.03.031.
[23] Qiu TX, Teo EC, Yan YB, Lei W. Finite element modeling of a 3D coupled foot-boot model. Med Eng Phys 2011;33:1228–33. https://doi.org/10.1016/j.medengphy.2011.05.012.
[24] Cho JR, Park SB, Ryu SH, Kim SH, Lee SB. Landing impact analysis of sports shoes using 3-D coupled foot-shoe finite element model. J Mech Sci Technol 2009;23:2583–91. https://doi.org/10.1007/s12206-009-0801-x.
[25] Kamal Z, Hekman EG, Verkerke JG. A combined musculoskeletal and finite element model of a foot to predict plantar pressure distribution A combined musculoskeletal and fi nite element model of a foot to predict plantar pressure distribution. Biomed Phys Eng Express 2024;10:035024. 10.1088/2057-1976/ad233d.
[26] Hannah I, Harland A, Price D, Schlarb H, Lucas T. Evaluation of a kinematically-driven finite element footstrike model. J Appl Biomech 2016;32:301–5. https://doi.org/10.1123/jab.2015-0002.
[27] Li S, Zhang Y, Gu Y, Ren J. Stress distribution of metatarsals during forefoot strike versus rearfoot strike: a finite element study. Comput Biol Med 2017;91:38–46. https://doi.org/10.1016/j.compbiomed.2017.09.018.
[28] Qian Z, Ren L, Ding Y, Hutchinson JR, Ren L. A dynamic finite element analysis of human foot complex in the sagittal plane during level walking. PLoS One 2013;8:1–10. https://doi.org/10.1371/journal.pone.0079424.
[29] Kim SH, Cho JR, Choi JH, Ryu SH, Jeong WB. Coupled foot-shoe-ground interaction model to assess landing impact transfer characteristics to ground condition. Interact Multiscale Mech 2012;5:75–90.
[30] Majdak M, Baranowski P, Małachowski J. Numerical studies of the energy absorption capacities and deformation mechanisms of 2D cellular topologies. Arch Civ Mech Eng 2024;5. https://doi.org/10.1007/s43452-024-00926-5.
[31] Płatek Pawełand Baranowski PJJ, Kucewicz M. Problems of deformation and damage studies of additively manufactured regular cellular structures. Handb Damage Mech Nano to Macro Scale Mater Struct, Springer International Publishing Cham 2022:215–47.
[32] Lakes RS. Design considerations for materials with negative Poisson's ratios. J Mech Des 1993;115:696–700. https://doi.org/10.1115/1.2919256.
[33] Mohammadi H, Ahmad Z, Petru M, Mazlan SA, Faizal Johari MA, Hatami H, et al. An insight from nature: Honeycomb pattern in advanced structural design for impact energy absorption. J Mater Res Technol 2023;22:2862–87. https://doi.org/10.1016/j.jmrt.2022.12.063.
[34] Yin H, Zhang W, Zhu L, Meng F, Liu J, Wen G. Review on lattice structures for energy absorption properties. Compos Struct 2023;304:116397. https://doi.org/10.1016/j.compstruct.2022.116397.
[35] Sun Y, Zhou Q, Niu W, Zhang S, Yick KL, Gu B, et al. 3D printed sports shoe Midsoles: enhancing comfort and performance through finite element analysis of negative Poisson's ratio structures. Mater Des 2024;245:113292. https://doi.org/10.1016/j.matdes.2024.113292.
[36] Leung MS, Yick KL, Sun Y, Chow L, Ng S. 3D printed auxetic heel pads for patients with diabetic mellitus. Comput Biol Med 2022;146:105582. https://doi.org/10.1016/j.compbiomed.2022.105582.
[37] Kucewicz M, Baranowski P, Małachowski J, Popławski A, Płatek P. Modelling, and characterization of 3D printed cellular structures. Mater Des 2018;142:177–89. https://doi.org/10.1016/j.matdes.2018.01.028.
[38] Kucewicz M, Baranowski P, Stankiewicz M, Konarzewski M, Płatek P, Małachowski J. Modelling and testing of 3D printed cellular structures under quasi-static and dynamic conditions. Thin-Walled Struct 2019;145:106385. https://doi.org/10.1016/j.tws.2019.106385.

[39] Cristiana M, Popescu D, Stochioiu C, Baciu F, Hadar A. Compressive behavior of thermoplastic polyurethane with an active agent foaming for 3D-printed customized comfort insoles. Polym Test 2024;137:108517. https://doi.org/10.1016/j.polymertesting.2024.108517.
[40] Iacob M, Popescu D, Alexandru TG. Printability Of thermoplastic polyurethane with low shore a hardness in the context of customized insoles production. UPB Sci Bull Ser D Mech Eng 2024;86:95–106.
[41] Iacob MC, Popescu D, Baciu F. Effect of process parameters on the hardness of 3D-printed thermoplastic polyurethane that includes foaming agent. Mater Plast 2023;60(144–54). https://doi.org/10.37358/MP.23.4.5694.
[42] Płatek P, Rajkowski K, Cieplak K, Sarzyński M, Małachowski J, Woźniak R, et al. Deformation process of 3D printed structures made from flexible material with different values of relative density. Polymers (Basel) 2020;12. https://doi.org/10.3390/POLYM12092120.
[43] Zhang S, Zhang Y, Zhang X, Yu C, Xu K, Qin J, et al. 3D-printed thermoplastic polyurethane/polyvinylidene fluoride gradient stiffness and hierarchical cellular structures with tailored energy absorption behavior. Addit Manuf 2024;83:104062. https://doi.org/10.1016/j.addma.2024.104062.
[44] Center, Toyota Labs R& D. Documentation: Total Human Model for Safety (THUMS) AM50 Pedestrian/Occupant Model Academic Version 4.02_20150527. 2015.
[45] Cheung JTM, Zhang M, Leung AKL, Fan YB. Three-dimensional finite element analysis of the foot during standing - a material sensitivity study. J Biomech 2005;38:1045–54. https://doi.org/10.1016/j.jbiomech.2004.05.035.
[46] Akrami M, Qian Z, Zou Z, Howard D, Nester CJ, Ren L. Subject-specific finite element modelling of the human foot complex during walking: sensitivity analysis of material properties, boundary and loading conditions. Biomech Model Mechanobiol 2018;17:559–76. https://doi.org/10.1007/s10237-017-0978-3.
[47] Burns GT, Gonzalez R, Zendler JM, Zernicke RF. Bouncing behavior of sub-four minute milers. Sci Rep 2021;11:1–15. https://doi.org/10.1038/s41598-021-89858-1.
[48] Yang Z, Cui C, Wan X, Zheng Z, Yan S, Liu H, et al. Design feature combinations effects of running shoe on plantar pressure during heel landing: a finite element analysis with Taguchi optimization approach. Front Bioeng Biotechnol 2022;10:1–13. https://doi.org/10.3389/fbioe.2022.959842.
[49] Wang Y, Li Z, Wong DW, Zhang M. Effects of ankle arthrodesis on biomechanical performance of the entire foot. PLoS One 2015;10:e0134340.
[50] Antunes PJ, Dias GR, Coelho AT, Rebelo F, Pereira T. Non-Linear Finite Element Modelling of Anatomically Detailed 3D Foot Model. 2008.
[51] Ozen M, Sayman O, Havitcioglu H. Modeling and stress analyses of a normal foot-ankle and a prosthetic foot-ankle complex. Acta Bioeng Biomech 2013;15:19–27. https://doi.org/10.5277/abb130303.
[52] Davia-Aracil M, Hinojo-Pérez JJ, Bertazzo M, Orgilés-Calpena E, Maestre-López MI, Llobell-Andrés C. Design and functionalisation of shoe outsoles with antimicrobial properties using additive manufacturing technologies: industrial applications. Comput Ind 2020;121. https://doi.org/10.1016/j.compind.2020.103246.
[53] Peng Y, Wang Y, Wong DW, Chen TL, Chen SF. Different Design Feature Combinations of Flatfoot Orthosis on Plantar Fascia Strain and Plantar Pressure : A Muscle-Driven Finite Element Analysis With Taguchi Method 2022;10:1–9. 10.3389/fbioe.2022.853085.
[54] Li Y, Leong KF, Gu Y. Construction and finite element analysis of a coupled finite element model of foot and barefoot running footwear. Proc Inst Mech Eng Part P J Sport Eng Technol 2019;233:101–9. https://doi.org/10.1177/1754337118803540.
[55] Uhao FMO, Unjie JLI, Ang ZUY, Hou SHZ, Ehr MIB. In Vivo Measurement of Plantar Tissue Characteristics and Its Indication for Foot Modeling 2019;47:2356–71. https://doi.org/10.1007/s10439-019-02314-0.
[56] Wang Y, Li Z, Wong DW. Finite element analysis of biomechanical effects of total ankle arthroplasty on the foot. J Orthop Transl 2018;12:55–65. https://doi.org/10.1016/j.jot.2017.12.003.
[57] Mao R, Guo J, Luo C, Fan Y, Wen J, Wang L. Biomechanical study on surgical fixation methods for minimally invasive treatment of hallux valgus 2017:1–6. https://doi.org/10.1016/j.medengphy.2017.04.010.
[58] Peng Y, Wong DW, Wang Y, Chen TL, Zhang G. Computational models of flatfoot with three-dimensional fascia and bulk soft tissue interaction for orthosis design. Med Nov Technol Devices 2021;9:100050. https://doi.org/10.1016/j.medntd.2020.100050.
[59] Giddins VL, Beaupre G, Whalen R, Carter D. Calcaneal loading during walking and running. Med Sci Sports Exerc 2010;32:627–34. https://doi.org/10.1097/00005768-200003000-00012.
[60] Lieberman DE, Venkadesan M, Werbel WA, Daoud AI, Dandrea S, Davis IS, et al. Foot strike patterns and collision forces in habitually barefoot versus shod runners. Nature 2010;463:531–5. https://doi.org/10.1038/nature08723.
[61] Song Y, Cen X, Chen H, Sun D, Munivrana G. The influence of running shoe with different carbon-fiber plate designs on internal foot mechanics: a pilot computational analysis. J Biomech 2023;153:111597. https://doi.org/10.1016/j.jbiomech.2023.111597.
[62] Mo F, Li Y, Li J, Zhou S, Yang Z. A three-dimensional finite element foot-ankle model and its personalisation methods analysis. Int J Mech Sci 2022;219:107108. https://doi.org/10.1016/j.ijmecsci.2022.107108.